Appl. Phys. B 34, 73–82 (1984)

Applied Physics B Photophysics and Laser Chemistry

Laser Irradiation of a Three-Level Gas System: Continued-Fraction Theory and Applications

R. Vilaseca, G. Orriols, and L. Roso

Departament de Física Fonamental, Universitat Autònoma de Barcelona, Bellaterra (Barcelona), Spain

R. Corbalán

Departamento de Optica, Universidad de Sevilla, Sevilla, Spain

E. Arimondo

Istituto di Fisica Sperimentale dell'Università di Napoli, Napoli, Italy and Gruppo Nazionale di Struttura della Materia, Sezione di Pisa, I-56100 Pisa, Italy

Received 4 November 1983/Accepted 22 January 1984

Abstract. The general steady-state solution of the density matrix equations for a Doppler broadened three-level system irradiated by two resonant standing-wave laser beams of arbitrary intensity is analyzed. The solution is expressed in a matrix continued fraction form, that involves 4×4 matrices in important configurations and is convenient for numerical computations. Some representative cases including the absorption spectra for a probe laser of arbitrary intensity, the Doppler-free multiphoton resonances and the optically pumped lasers are analyzed numerically in connection with previous experimental investigations.

PACS: 42.65, 32, 33

In quantum optics and nonlinear spectroscopy the interaction of two electromagnetic fields with transitions sharing a common level, i.e. a three-level system, is dealt with very often. The two-photon transitions, the optically pumped lasers, the double-resonance experiments, the sideband or multimode laser spectroscopy are examples of the three-level configuration [1]. The electromagnetic fields may be composed by travelling waves (TW) or standing waves (SW), and different phenomena are encountered when these waves interact with homogeneously or inhomogeneously broadened absorption lines. For homogeneous lines the theoretical analysis is straightforward and the spatial inhomogeneity of a SW electric field may be included through a spatial integration [2]. For Doppler inhomogeneously broadened systems the presence of a velocity distribution produces new phenomena, but simultaneously leads to a more intrincate analysis. The TW configuration is well known with the solution of the three-level density matrix equations expressed in a closed analytical form. The Autler-Townes effect and the asymmetry for copropagating or counterpropagating waves are the main features well investigated experimentally [3–6]. SW configurations occur typically in the experiments inside the laser optical cavity. Velocity-tuned multiphoton transitions are the characteristic phenomena occurring in the SW, as analized in a few experiments [7–10]. The theoretical analysis for the SW interaction of moving absorbers leads to an infinite set of coupled difference equations for the spatial components of the density matrix elements, whose solution must be handled by a computer. A general solution of the three-level problem, valid for whichever TW and SW combinations of the electromagnetic fields, will be presented in this paper on the basis of the matrix continued fraction formalism. With such a numerical algorithm the amount of computation is greatly re-

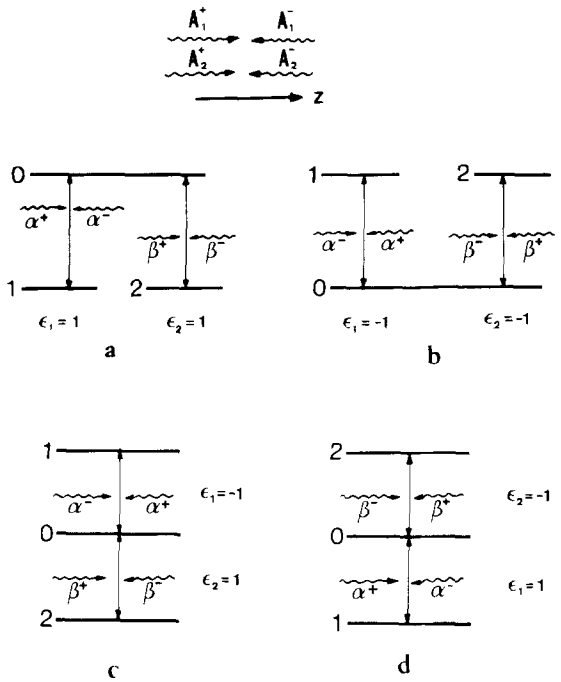

Fig. 1a–d. Configurations treated with the formalism of this paper. The definition of the Rabi flopping frequencies $\alpha^{\pm}$ and $\beta^{\pm}$ depending on the configuration following (12), is shown in the figure on the basis of the travelling waves $A_1^{\pm}$ and $A_2^{\pm}$ choice presented in the top of the figure

duced as compared to the straight numerical solution of the difference equations.

The continued fraction solution applied for the first time to a single SW laser mode [11, 12] was extended by Sargent and coworkers [13] and generalized to matrices by Bambini [14] in the interaction between a multimode laser and a system of stationary absorbers. Recurrence relations for infinite dimensional matrices were introduced in [15] for multimode gas lasers. For a three-level system Feldman and Feld [16] presented a continued fraction solution of complex numbers valid for a weak TW probe beam and an arbitrary intensity SW pump. However, important cases of the three-level laser spectroscopy as the optically pumped gas lasers or the gas lasers simultaneously oscillating on two transitions sharing a common level cannot be adequately described by that solution. If in the case of an optically pumped ring laser the pump and the pumped laser are TW, in the most common lasers a SW pumped beam occurs, while the pump wave may be strongly attenuated in the forward-backward propagations. In the lasers simultaneously oscillating on two transitions, two SW are present. This last case has been analyzed by Paxton and Milonni [17] through a numerical solution of the infinite set of difference recurrence relations satisfied by the spatial components of the density matrix.

In this paper we show that in the most general case of an arbitrary relation between the wavelengths of the two electromagnetic fields the solution is expressed through matrices of infinite dimension, and this formalism would not provide any real computational advantage. Instead, if we suppose, without loss of generality, that the wavenumbers of the electromagnetic fields are in the ratio of integer numbers, the solution depends on matrices of finite dimension. Moreover, it will be shown that the following important configurations may be solved through continued fractions of 4×4 matrices: i) the electromagnetic fields have the same wavenumber; ii) a SW and TW of arbitrary intensity are applied; iii) the Doppler broadening of one of the transitions can be neglected.

Because some features in the three-level absorption signals depend on the extension of the limits in the Doppler velocity integration, Kyrölä and Salomaa in [18] have provided approximate solutions for the density matrix to be used in the Doppler integration. The continued fraction solution has allowed us to make a more detailed analysis of several features appearing in the three-level spectroscopy.

In a set of recent experiments [19] the three-level saturation spectroscopy has been applied to probe with high accuracy the relaxation processes produced by the velocity-changing and phase-interrupting collisions. We will not include in our analysis the velocity-changing effects on the populations, but a decay rate of the coherences produced by the phase-interrumping collisions will be introduced.

The paper is organized as it follows: after a schematic presentation of the theoretical problem, the matrix continued fraction solution is developped in Sect. 1. In Sect. 2 numerical calculations are presented with reference to experimental configurations of three-level systems. Thus we will analise the TW and SW probe absorption of an infrared molecular vibrational transition, in presence of pumping on an adjacent vibrational transition [7]. The Doppler-free two-photon absorptions and three-photon cross-resonances for molecular electronic transitions will be examined [8, 9]. Finally an optically pumped Raman laser operating on excited levels of neon and the dips in its output power at high pump will be investigated [20]. The lineshapes of the absorption or emission spectra observed in those experiments will be reproduced and unexplored features will be presented.

1. Theory

1.1. Three-Level System and Motion Equations

The three-level configurations under consideration are shown in Fig. 1, with the common level 0 coupled to

levels 1 and 2 by electric dipole matrix elements $\boldsymbol{\mu}_{01}$ and $\boldsymbol{\mu}_{02}$, respectively. Let denote the energy of level j by W_j and define $W_j - W_K = \hbar w_{jk}$. If we introduce

$$\varepsilon_1 = \mathrm{sign}(\omega_{01}) \qquad \varepsilon_2 = \mathrm{sign}(\omega_{02}) \tag{1}$$

these quantities may be used to label each of the level configurations of Fig. 1, so that they will be treated by a single formalism. Thus for the inverted-V configuration (Fig. 1a) $\varepsilon_1 = +1$, $\varepsilon_2 = +1$; for the V configuration (Fig. 1b) $\varepsilon_1 = -1$, $\varepsilon_2 = -1$; for the cascades $\varepsilon_1 = +1$, $\varepsilon_2 = -1$ or $\varepsilon_1 = -1$, $\varepsilon_2 = +1$.

The absorbers are subjected to relaxation processes which will be phonomenologically accounted for by damping constants. The total population relaxation rates $\gamma_j (j = 0, 1, 2)$ are composed by the decay rates Γ_j to levels not included in the three-level system under examination and the rates Γ_{ji} for the spontaneous decay or collisional population transfer from level i to level j. Repopulation of level i from external levels to the system is described by the population rate $\lambda_i(v)$ which depends on the velocity v along the laser propagation axis z. For the coherences, besides the above relaxation processes, we introduce a rate γ_{ij}^c in general a complex number, to take into account the influence of finite-bandwith laser effects and/or phase-interrupting collisions. Thus the time evolution of the ensemble-averaged density matrix $\varrho(v, z, t)$ under the action of relaxation processes is described by

$$\frac{\partial}{\partial t}\varrho_{jj}(v,z,t)\bigg|_{\text{relax.}} = -\gamma_j \varrho_{jj} + \sum_{i \neq j} \Gamma_{ji}\varrho_{ii} + \lambda_j(v), \tag{2a}$$

$$\frac{\partial}{\partial t}\varrho_{ij}(v,z,t)\bigg|_{\text{relax.}} = -\gamma_{ij}\varrho_{ij}, \tag{2b}$$

with $i, j, k = 0, 1, 2$ and

$$\gamma_j = \Gamma_j + \sum_{i \neq j} \Gamma_{ij}, \tag{3a}$$

$$\gamma_{ij} = (\gamma_i + \gamma_j)/2 + \gamma_{ij}^c; \qquad \gamma_{ij} = \gamma_{ji}^*. \tag{3b}$$

The equilibrium population densities $\varrho_{jj}^0(v)$ in absence of applied fields are determined by the steady-state solution of (2), and it results

$$\lambda_j(v) = \gamma_j \varrho_{jj}^0(v) - \sum_{i \neq j} \Gamma_{ji}\varrho_{ii}^0(v). \tag{4}$$

The $\varrho_{jj}^0(v)$ will be expressed as

$$\varrho_{jj}^0(v) = N_j^0 G(v) \tag{5}$$

with $G(v)$ a standard Maxwellian velocity distribution, whose most probable velocity is denoted u.

The two monochromatic electromagnetic fields $\mathbf{E}_1(z, t)$ and $\mathbf{E}_2(z, t)$ propagating along the z axis with angular frequencies $\Omega_1, \Omega_2 > 0$, are described by

$$\mathbf{E}_i(z,t) = \sum_{\mu = \pm 1} A_i^\mu \{\mathbf{e}_i \exp[-\mathrm{i}(\Omega_i t - \mu k_i z)] + \text{c.c.}\}/2 \quad (i = 1, 2), \tag{6}$$

where the index μ describes the counterpropagating components whose intensities may be different one from the other. We shall assume that by the choice of the polarization vectors $\mathbf{e}_1$ and $\mathbf{e}_2$ or of the frequency difference $|\Omega_1 - \Omega_2|$ the field $\mathbf{E}_1$ drives the 0–1 transition only and $\mathbf{E}_2$ the 0–2 transition only. We define the detunings for nonmoving absorbers by

$$\Delta_i = \varepsilon_i(\Omega_i - |\omega_{0i}|) \quad (i = 1, 2) \tag{7}$$

and in the solution we will introduce $\Delta_0 = 0$.

The time evolution of the density matrix elements is given by

$$\left(\frac{\partial}{\partial t} + v\frac{\partial}{\partial z}\right)\varrho_{ij}(v,z,t) = (i\hbar)^{-1}[H(z,t), \varrho(v,z,t)]_{ij} + \frac{\partial}{\partial t}\varrho_{ij}(v,z,t)\bigg|_{\text{relax.}} \tag{8}$$

with the following Hamiltonian matrix elements

$$H_{jj} = W_j \quad (j = 0, 1, 2)$$

$$H_{0i}(z,t) = -\sum_{\mu = \pm 1} A_i^\mu \boldsymbol{\mu}_{0i} \cdot \{\mathbf{e}_i \exp[-\mathrm{i}(\Omega_i t - \mu k_i z)] + \text{c.c.}\}/2 \quad (i = 1, 2). \tag{9}$$

The standard rotating-wave approximation (RWA) is applied to the solution of (8), and the leading terms in the electromagnetic field absorber interaction will be expressed through the following flopping frequencies, assumed to be real numbers without any loss of generality:

$$\alpha^\mu = (2\hbar)^{-1}\boldsymbol{\mu}_{01} \cdot (\mathbf{e}_1 A_1^\mu \delta_{\varepsilon_1, 1} + \mathbf{e}_1^* A_1^{-\mu}\delta_{\varepsilon_1, -1}), \tag{10a}$$

$$\beta^\mu = (2\hbar)^{-1}\boldsymbol{\mu}_{02} \cdot (\mathbf{e}_2 A_2^\mu \delta_{\varepsilon_2, 1} + \mathbf{e}_2^* A_2^{-\mu}\delta_{\varepsilon_2, -1}), \quad (\mu = \pm 1). \tag{10b}$$

Depending on the level configuration the $\alpha^\pm$, $\beta^\pm$ frequencies are associated to the different waves in the form indicated in Fig. 1.

The steady state solution of (8) can be obtained introducing for the density matrix elements a two-index Fourier expansion with k_1 and k_2 fundamental spatial frequencies [17]. However, this expansion can be simplified if we suppose, without loss of generality, that two integers a and b can be defined such that a/b is a rational number and

$$k_1 = ak, \qquad k_2 = bk, \tag{11}$$

where k is a reduced wavenumber. Then the steady-state solution of (8) becomes the one-index expansion:

$$\varrho_{ij}(v,z,t)=\exp[\mathrm{i}(\varepsilon_i\Omega_i-\varepsilon_j\Omega_j)t]\sum_{q=-\infty}^{+\infty}P_{ij}^q(v)\exp(\mathrm{i}qkz)$$
$$(i,j=0,1,2), \tag{12}$$

where $\varepsilon_0=0$ has been introduced and an infinite number of two-index coefficients have been grouped in each $P_{ij}^q(v)$ coefficient. From the Hermitian conjugate relation for the density matrix elements it turns out that

$$P_{ij}^q=(P_{ji}^{-q})^* \tag{13}$$

for any integer q. Furthermore, by substituting (12) into (8) it results

$P_{jj}^q=0$ for any j, if q is an odd integer number.

$P_{10}^q=P_{01}^q=0$ if q and a are not both even or odd numbers.

$P_{20}^q=P_{02}^q=0$ if q and b are not both even or odd numbers.

$P_{12}^q=P_{21}^q=0$ if q and $a+b$ are not both even or odd numbers.

As standard in the steady-state solution of laser problems the relations between the Fourier components P_{ij}^q are obtained by picking out the same spatial dependence at the right- and left-hand sides of (8). In the resulting relations we introduce the Fourier components of the population differences

$$D_i^q=P_{00}^q-P_{ii}^q, \tag{14}$$

and we eliminate the optical coherences making use of

$$P_{10}^q=\mathrm{i}L_{10}^q\sum_{\mu=\pm1}(\alpha^\mu D_1^{q+\mu a}-\beta^\mu P_{12}^{q+\mu b})$$
$$P_{20}^q=\mathrm{i}L_{20}^q\sum_{\mu=\pm1}(\beta^\mu D_2^{q+\mu b}-\alpha^\mu P_{21}^{q+\mu a}), \tag{15}$$

where

$$(L_{jl}^q)^{-1}=\gamma_{jl}+\mathrm{i}[(\Delta_j-\Delta_l)+qkv].$$

Thus we get a set of recurrence relations involving D_1^q, D_2^q, P_{12}^q, and P_{21}^q only. From these variables through (15) the Fourier components of the optical coherences are derived. The complexity of the problem has been greatly reduced by this procedure. The Fourier components of the population differences $\varrho_{00}-\varrho_{ii}$ or of the ϱ_{12} and ϱ_{21} coherences only cannot be eliminated anymore without destroying the simplicity of the recurrence relations.

The recurrence relations for D_1^q, D_2^q, P_{12}^q, and P_{21}^q may be written as

$$F_q^0X^q+\sum_{\mu=\pm1}(G_q^\mu X^{q+2\mu a}+H_q^\mu X^{q+2\mu b}$$
$$+K_q^\mu X^{q+2\mu(a-b)})=J^0\delta_{q,0}, \tag{16}$$

where the four-components vectors X^q and J^0 are defined by

$$X^q\equiv(D_1^q, D_2^q, P_{12}^{q+a-b}, P_{21}^{q-a+b})$$
$$J^0\equiv(\Lambda_1,\Lambda_2,0,0) \tag{17}$$

and where

$$\Lambda_i=M_i^0\lambda_0-M_0^0\lambda_i \quad (i=1,2)$$
$$M_j^q=\gamma_j-\sum_{j\neq l}\Gamma_{jl}+\mathrm{i}qkv \quad (j=0,1,2).$$

The elements of the 4×4 matrices F_q^0, $G_q^{\pm1}$, $H_q^{\pm1}$, and $K_q^{\pm1}$ are reported in the appendix. The X^q are different from zero only for q even integer numbers.

In interpreting the numerical results it is convenient to make use of a property that extensively applied in previous analyses of the three-level spectroscopy, may be generalized to the case of four strong electromagnetic waves. The source terms Λ_i can be expressed as

$$\Lambda_i=A_i(N_0^0-N_i^0)G(v)+B_i(N_0^0-N_2^0)G(v) \tag{18}$$

with the coefficients A_i and B_i, independent from α^μ and β^μ, presented in the Appendix. Thus the solution of (16) may be obtained summing up the solutions with $(N_0^0-N_1^0)=0$ or $(N_0^0-N_2^0)=0$. Finally, note also that for given values of the parameters $N_0^0-N_1^0$, $N_0^0-N_2^0$, $\alpha^\pm$, $\beta^\pm$, Δ_1, Δ_2 and the relaxation rates, a three-level solution can be applied to any configuration depicted in Fig. 1 by interpreting the Δ_1 according to (7) and using the relation (10) between the $\alpha^\pm$ ($\beta^\pm$) and the TW $A_1^\pm$ ($A_2^\pm$), schematically shown in Fig. 1.

1.2. Continued-Fraction Solution

The system of Eq. (16) with a recurrence relation connecting seven vectors X^q, may be written as connecting three vectors if we introduce vectors and matrices of dimension 4θ, θ being the largest one of the a and b numbers.

We have found that several important configurations may be solved through a recurrence relation involving vectors and matrices with the minimum dimension, i.e., dimension 4. An important case is when the wave numbers k_1 and k_2 may be supposed equal. This occurs in laser spectroscopy on V or inverted $-$V configurations when the splitting ω_{12} lies in the radiofrequency or microwave regions. In effect, if $|k_1-k_2|$ is much smaller than the inverse of the distance Δz covered by the absorbers with velocity v during the interaction

time with the electromagnetic fields, the difference in the spatial modulations of the two electromagnetic fields can be neglected. With $k_1 = k_2$ (16) may be written as

$$W_q^{-1} X^{q-2} + W_q^0 X^q + W_q^{+1} X^{q+2} = J^0 \delta_{q,0}, \tag{19a}$$

where

$$W_q^0 = F_q^0 + \sum_{\mu=\pm 1} K_q^\mu$$
$$W_q^{\pm 1} = G_q^{\pm 1} + H_q^{\pm 1}. \tag{19b}$$

This recurrence relation is formally identical to those derived in [11] for complex numbers and in [14, 15] for matrices, and the solution may be written as

$$X^0 = (W_0^{-1} Z_{-2}^{-1} + W_0^0 + W_0^{+1} Z_{+2}^{+1})^{-1} J^0, \tag{20a}$$

$$X^q = Z_q^{\pm 1} X^{q \mp 2} \tag{20b}$$

with the matrix continued fractions $Z_q^\mu (\mu = \pm 1)$ given by

$$Z_q^\mu = -(W_q^0 + W_q^\mu Z_{q+2\mu}^\mu)^{-1} \cdot W_q^{-\mu} = -\cfrac{1}{W_q^0 - W_q^\mu \cfrac{1}{W_{q+2\mu}^0 - W_{q+2\mu}^\mu \cfrac{1}{W_{q+4\mu}^0 - \ddots}\, W_{q+4\mu}^{-\mu}}\, W_{q+2\mu}^{-\mu}}\, W_q^{-\mu}. \tag{20c}$$

Similar recurrence relations are obtained if we suppose that an electromagnetic field is composed by a travelling wave, i.e. for instance $\beta^- = 0$. Thus it results, for any value of k_1/k_2,

$$H_q^\pm = K_q^\pm = 0 \quad \forall q \tag{21}$$

and the recurrence relation becomes

$$G_q^{-1} X^{q-2a} + F_q^0 X^q + G_q^{+1} X^{q+2a} = J^0 \delta_{q,0} \tag{22}$$

to be solved with the formalism of (20).

Another important particular case appears for $k_2 \simeq 0$, i.e. when the spatial modulation of the $\mathbf{E}_2$ field is not experienced by the absorbers. Thus the Doppler broadening of the 0–2 transition is negligible, as for a radiofrequency, microwave or long-wavelength far-infrared transition. If $k_2 \simeq 0$ the two counter-propagating components β^+ and β^- cannot be distinguished and this case is formally equivalent to that of a travelling wave with an amplitude such that its flopping frequency is $\beta^+ + \beta^-$.

The continued fractions (20) are evaluated numerically by truncation to a finite number of terms in the denominator. It is a standard procedure in the calculation to check if the addition of one term in the denominator modifies the numerical value within the required accuracy. In calculating space-averaged observables, nonvanishing contributions arise only from the Fourier coefficients whose spatial oscillation matches the coupled field. For instance, the absorbed power from the $\beta^\pm$ component of the $\mathbf{E}_2$ field, space-, time- and velocity-averaged, is given by

$$P_{\text{abs}}^{2\pm} = -2\varepsilon_2 \hbar \Omega_2 \beta^\pm \langle \text{Im}\{P_{20}^{\mp b}\} \rangle_v v, \tag{23}$$

where $\langle\ \rangle_v$ denotes the velocity integration. Notice that if the two-index Fourier expansion would have been used instead of (12), then the infinite number of coefficients grouped in $P_{20}^{\mp b}$ should have been calculated explicitely.

For two SW with k_1/k_2 attaining a nontrivial value the above formalism would be not manageable as high-dimension matrices must be handled. However a first insight into the basic physics of the phenomena could be get by approximating the actual k_1/k_2 ratio by a similar a/b ratio with small a and b integers. The conditions for the validity of this approximation are that the changes introduced in the Doppler shifts experienced by the absorbers and in the phase matching conditions existing between the waves be negligible, i.e. $\Delta k_i < \gamma/u$ and $\Delta k_i < \pi/2L$ respectively, where Δk_i represents the error introduced in the wavenumber k_i and L the cell length.

2. Numerical Results

The solution of Sect. 1 allows to compute numerically the absorber response in any three-level experiment, and a few applications of the theoretical analysis will be here presented.

2.1. Probe Spectroscopy

A large amount of spectroscopic information has been derived from the experiments where the influence of a strong pump laser on a Doppler-broadened transition is monitored on a three-level scheme by a laser resonant on an adjacent transition. The weak-probe spectroscopy in the case of a SW pump is interpreted within the Feldman and Feld [16] treatment where a series expansion of the density matrix elements in the probe intensity is restricted to the lowest order. However, in order to analyse properly the probe response it is important to derive the influence of the probe intensity, as it may be obtained on the basis of the matrix continued fraction solution.

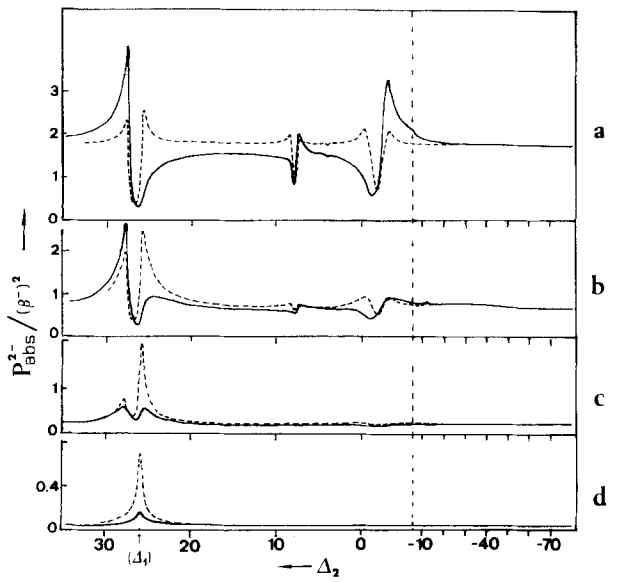

Fig. 2a–d. The β^- relative absorbed power (measured in the same arbitrary units) plotted versus the Δ_2 detuning at different values of the probe field. From top to bottom figures, the following β^- values have been chosen: 0.005, 0.25, 1, and 5 MHz, respectively. The dashed lines correspond to a TW probe, the continuous lines to a SW probe. Parameters are in the text. Notice that for $\Delta_2 < -6$ MHz, on the right side of the horizontal axis, a different horizontal scale was used in order to make more evident the features of that region

A significative example of the three-level probe spectroscopy is represented by the infrared laser intracavity experiments on methyl-fluoride molecules by Reid and Oka [7] where two CO_2 lasers oscillating on the same line but with orthogonal polarizations were used as pump and probe beams. Multiphoton processes and other peculiar features produced by the SW pump laser were observed, as discussed in [21]. In this experiment the same wavenumber k results for the pump and probe fields, so that a 4×4 matrix continued fraction solution applies. The values of the parameters, appropriate to the experimental conditions and expressed in true, not angular, frequencies were: $\gamma_0=\gamma_1=\gamma_2=0.2$ MHz, $\gamma^c_{ij}=\Gamma_{ij}=0\,(\forall_{i,j})$, intensity for the pump 0–1 transition $\alpha^+=\alpha^-=5$ MHz and pump detuning $\Delta_1=26$ MHz. However at variance with the experiment in our numerical analysis we have introduced the initial population $N^0_0-N^0_1=0$, $N^0_0-N^0_2=-1$ and the Doppler width $Ku=10^4$ MHz. This choice of the initial population allows a direct study of the coherent effects, and the inclusion of a very large Doppler broadening allows to analyse in the spectrum the features produced by absorbers with large Doppler shift, thus extending the investigation of Kyrölä and Salomaa [18]. Figure 2 represents the power P^{2-}_{abs} absorbed from the β^- of the $\mathbf{E}_2$ probe field [23], normalized to the $(\beta^-)^2$ incident power. From Fig. 2a–d the intensity of the probe beam takes progressively higher values. In the figures the dashed lines represent the case of a TW probe ($\beta^+=0$) and the continous lines describe the case of a SW probe ($\beta^+=\beta^-$).

For the case of a weak probe laser (Fig. 2a) the resonant features which appear at $\Delta_2\simeq0$ and $\Delta_2=\Delta_1/(2n+1)$, $n=0,1,2,\ldots$ for a TW probe are produced by multiphoton processes involving β^- photon: the $\beta^-\alpha^\pm\alpha^\mp$ three-photon process (among others of higher order) for the $\Delta_2\simeq0$ feature, the $\beta^-\alpha^-$ two-photon one for $\Delta_2\simeq\Delta_1$, the $\beta^-\alpha^-\alpha^+\alpha^-$ four-photon one for $\Delta_2\simeq\Delta_1/3$, etc. For each feature the two-peaks structure is a consequence of an increase in the number of resonating absorbers, whereas the dip is produced by the absence of such absorbers, as explained in detail with the model of the dressed atom applied to the SW pump case [22]. In the case of a SW probe it appears that one peak in every feature increases its intensity by a factor 2, whereas the other peak disappears, leading to a dispersive shape of the signals. This behaviour arises from an interference effect either constructive or destructive between the polarizations induced in the medium by each counter-propagating component of the SW probe wave.

Figure 2b–d show that by increasing the probe intensity the background signal in the probe absorption decreases, as in absence of the pump laser, with a $(1+G)^{-1/2}$ dependence, $G=4(\beta^-)^2/\gamma_0\gamma_2$ being the saturation parameter of the 0–2 transition. Moreover, all the resonant features associated with the SW character of the pump are smeared out, except that corresponding to $\Delta_2=\Delta_1$. This behaviour cannot be described through the dressed-system energy diagram of [22], which is applicable at weak probe intensity only, but that analysis allows us to interpret qualitatively this dependence on the probe intensity when probe saturation is also considered. The $\Delta_2\simeq0$ and $\Delta_2\simeq\Delta_1/3$ features and the second peak of the $\Delta_2\simeq\Delta_1$ feature disappear at medium probe intensities because they are created by low-velocity absorbers near-resonant with β^- wave and suffer strong saturation broadening. On the contrary, the first peak of the $\Delta_2\simeq\Delta_1$ feature is produced by a two-photon Raman process involving high-velocity absorbers not resonant with the β^- wave. In effect the strenght of this peak is strongly dependent on the extension of the Doppler width. This Raman peak is less affected by the power broadening and in consequence it emerges clearly from the background and its center approachs to $\Delta_2=\Delta_1$, with increasing the probe intensity. All this behaviour with the probe intensity applies also for the SW case, because it is independent from the presence of the interference phenomena described above.

This overall saturation behaviour applies also to the $\Delta_2 \simeq -\Delta_1$ and $\Delta_2 \simeq \Delta_1/3$ resonances, clearly noticeable in Fig. 2b. They are produced by the $\beta^-\alpha^+$ and $\beta^-\alpha^+\alpha^-\alpha^+$ multiphoton processes, respectively, and are supported by a very limited velocity group of absorbers.

In the SW case at large probe intensities a Lamb dip centered at $\Delta_2 = 0$ would be expected to appear, but due to its small contrast and high width [12] it is completely masked by the features induced near $\Delta_2 = 0$ by the SW pump field.

Finally it should be mentioned that adopting a limited Doppler width all the spectral structure shown in Fig. 2 remains almost unchanged except the first peak of the $\Delta_2 \simeq \Delta_1$ feature, which will be significantly reduced because only absorbers with $|kv| \gg \alpha$ contribute to it [22].

2.2. *Doppler-Free Multiphoton Resonances in a Standing-Wave*

In the previous subsection we have analized the signals produced by the velocity-tuned multiphoton transitions with the frequency of the pump laser fixed and the frequency of the probe laser swept over the Doppler broadened absorption profile. Three-level velocity-tuned resonances occur also in the experiments where a single laser is coupled to both 0–1 and 0–2 transitions, and by tuning the laser frequency the populations and coherences of both transitions are simultaneously modified. In the experiments of this kind reported in the literature [8, 9] the laser was composed by two counter-propagating waves and this configuration will be analised here. In the framework of our description this case corresponds to the equations of Sect. 1 assuming $\Omega_1 = \Omega_2 = \Omega$, $k_1 = k_2 = k$ and both $\alpha^{\pm}$ and $\beta^{\pm}$ different from zero. The flopping frequencies α^{ε_1}, β^{ε_2} depend on the intensity of one TW component of the laser, while $\alpha^{-\varepsilon_1}$, $\beta^{-\varepsilon_2}$ depend on the other one.

The general solution of Sect. 1 with 4×4 matrices is required when none of these flopping frequencies is small enough to be teatred as a perturbation. This applies for instance to a Doppler-free two photon absorption with the two counterpropagating waves equal in intensity, as in the experiment on Na_2 by Woerdman and Shuurmans [8]. In that work a three-level cascade configuration, as in Fig. 1d, has been involved. As typical of Doppler-free two-photon transitions we define

$$\omega_{01} = \omega_0 - \delta, \quad \omega_{20} = \omega_0 + \delta,$$

where ω_0 is the laser frequency for the two-photon transition, $-\delta$ and $+\delta$ are the detunings from that frequency for the one-photon 0–1 and 2–0 transitions,

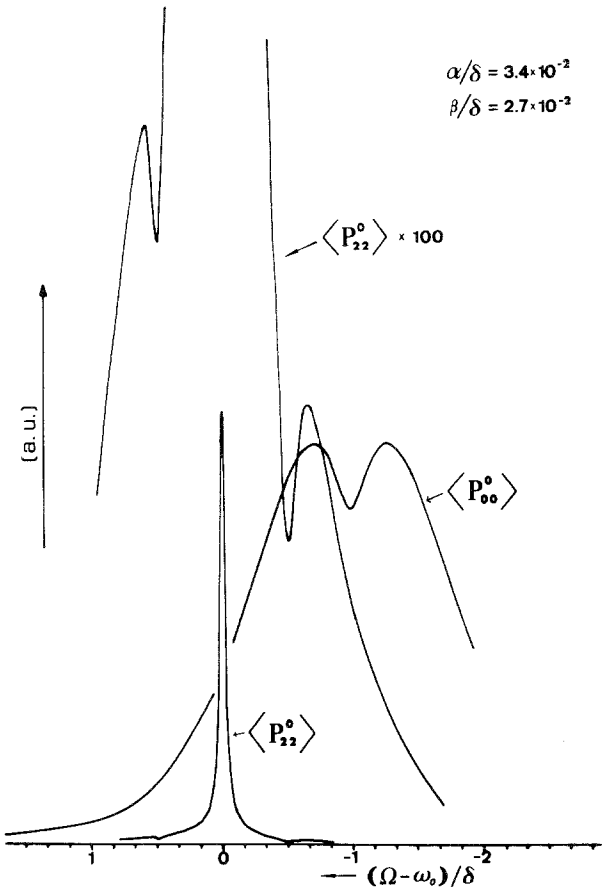

Fig. 3. The velocity integrated $\langle P^0_{22} \rangle$ and $\langle P^0_{00} \rangle$ populations versus $(\Omega - \omega_0)/\delta$, the normalized laser detuning from the two-photon resonance for the conditions of the experiment of [8]. Different arbitrary units have been used for the $\langle P^0_{22} \rangle$ and $\langle P^0_{00} \rangle$ populations. Fine details of the $\langle P^0_{22} \rangle$ population have been reported on the upper curve on a scale expanded vertically by 100 times

respectively. We have obtained a numerical solution of the density matrix equations with the following values of the parameters, taken from [8]: $\Gamma_0/\delta = 1.4 \times 10^{-2}$, $\Gamma_1/\delta = 1.0 \times 10^{-3}$, $\Gamma_2/\delta = 3.1 \times 10^{-3}$, $\gamma^c_{01}/\delta = 1.1 \times 10^{-2}$, $\gamma^c_{02}/\delta = 1.0 \times 10^{-2}$, $\gamma^c_{12}/\delta = 3.5 \times 10^{-2}$ and $ku/\delta = 0.84$. The relaxation rates γ^c_{ij} for the coherences have been introduced to describe the finite-bandwith laser excitation, and the initial population has been concentrated in the lower level. Because δ is comparable to the Doppler width the one-photon and two-photon transitions are nearly simultaneously resonant. In the experiment the space-averaged fluorescence intensity originated from the levels 0 and 2 was observed versus the laser frequency, and as these signals depend on the populations $\langle P^0_{00} \rangle$ an $\langle P^0_{22} \rangle$, we have reported these quantities in Fig. 3. The $\langle P^0_{00} \rangle$ spectrum shows a Doppler profile produced mainly by the one-photon transition $1 \rightarrow 0$, with a Lamb dip at the center of the

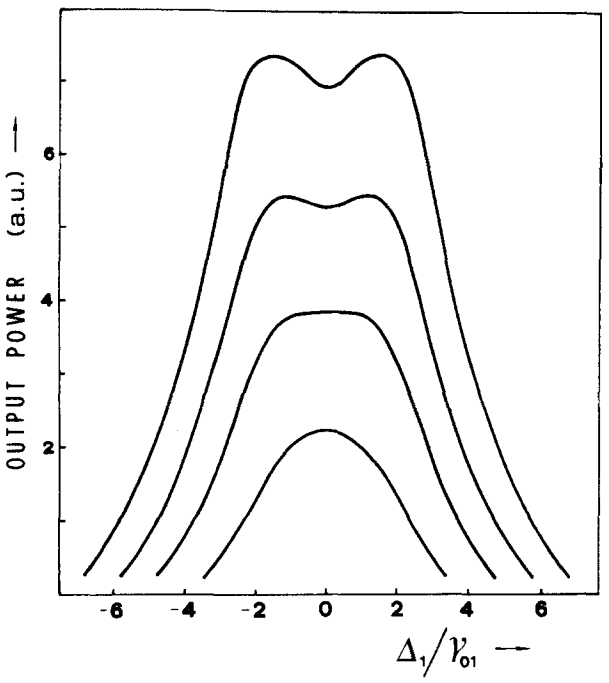

Fig. 4. Representation of the Raman laser output power versus tuning for a pump laser on resonance in the conditions of [20]. Curves from bottom to top are obtained for $C=3.13$, 4.40, 5.50, and 6.76, respectively

Doppler profile produced by the simultaneous saturation of the $1\rightarrow 0$ transition by the counterpropagating waves. The $\langle P_{22}^0\rangle$ population, created by the two-photon $1\rightarrow 2$ transition, presents a Doppler-broadened pedestal superimposed by the narrow Doppler-free signal originated at $\Omega=\omega_0$ by the absorption of two counterpropagating photons. The $\langle P_{22}^0\rangle$ spectrum presents also two dips at $\Omega=\omega_0-\delta/2$ and $\Omega=\omega_0+\delta/2$ produced by three-photon cross-resonances between one- and two-photon processes.

By a comparison of Fig. 3 with the experimental curves of [8] it appears that our numerically constructed lineshapes provide a precise description of the whole experimental results. While a perturbation analysis has been used previously to describe the position of the saturation resonances observed in the experiment and their main features [23], the lineshape can be obtained only through an high intensity treatment as our matrix continued fraction solution.

2.3. *Optically Pumped Gas Lasers*

In this important case of the three-level Λ-folded system, laser pumping occurs on a transition and laser emission is originated from a transition sharing the upper level with the first one. The Raman process, which is inherent in this coherently excited system, is a convenient method to achieve a continuous tunability of the laser output. Baklanov et al. [20], who to our knowledge reported the first operation of a resonant Raman laser, investigated theoretically the output characteristics, with an analysis that was restricted to the hypothesis of low gain and they did not reproduced the experimental conditions. Moreover most laser analyses reported in the literature were restricted to the calculation of the gain in the TW case.

We will analyse the experimental results of [20] on the basis of the matrix continued fraction solution. In the Λ-folded configuration of Fig. 1 for the $2p_4-2s_2-2p_1$ levels of Ne atoms, the 2–0 transition was pumped by a TW beam at 1.52 μm with a constant amplitude β^-, and the SW emission ($\alpha^+=\alpha^-$) at 1.15 μm was observed on the coupled 0–1 transition. In the experiment a narrow resonance dip was observed in the output power of the laser versus the frequency tuning, and it was interpreted on the basis of the saturation of the two-quantum 2–1 transition, with a width $(\gamma_1+\gamma_2)/2$ typical of the Raman process.

In the Λ-folded configuration a well known anisotropy exits for the 0–1 gain of the SW components parallel and antiparallel with respect to the TW pump laser. If we impose that the laser oscillation at the Ω_1 frequency occurs in a SW configuration, the self consistent equations for the steady state regime of the laser system are written as [24]:

$$\begin{aligned} Q^{-1} &= -4\pi \operatorname{Im}\{\chi_1\} \\ \Omega_1-\Omega_c &= -2\pi\Omega_1 \operatorname{Re}\{\chi_1\}, \end{aligned} \tag{24}$$

where Q and Ω_c represent respectively the quality factor and the resonant frequency of the laser cavity, and where χ_1, the electric susceptibility of the Ne atoms at the laser frequency, is given by

$$\chi_1(\alpha^+=\alpha^-,\Omega_1)=\boldsymbol{\mu}_{01}\cdot\mathbf{e}_1\langle P_{01}^a+P_{01}^{-a}\rangle_v/A_1, \tag{25}$$

where $\langle\ \rangle_v$ denotes an integration over the velocity distribution. Forward-backward anisotropy in the gain is included in the laser resonant conditions through this definition. A numerical analysis of (24, 25) was performed for the following parameters, derived from [20] and typical of this Raman laser operation: $\gamma_0/\gamma_{01}=1.5$, $\gamma_1/\gamma_{01}=0.5$, $\gamma_2/\gamma_{01}=0.7$, $\gamma_{ij}^c=\Gamma_{ij}=0\,(\forall i,j)$, $k_1/k_2=a/b=4/3$, $k_1u/\gamma_{01}=36$, $\beta^-/\gamma_{01}=1.5$. In the analysis we have assumed that the incoherent pumping mechanism of the discharge populates the level 2 only: $N_2^0\neq 0$ and $N_1^0=N_0^0=0$, because in the Raman laser oscillation is achieved in the absence of population inversion. Moreover we have verified that the Raman gain requires $N_1^0/N_2^0<1$. The selfconsistent Equations (24, 25) were solved introducing the appropriate sus-

ceptibility function derived from the density matrix equations.

For the range of parameters introduced into the numerical analysis the frequency pulling resulted negligible and the laser frequency Ω_1 equal to Ω_c, the cavity frequency. The other relevant laser quantity, the laser output power, was plotted in Fig. 4 versus the laser detuning from the atomic transition frequency. The curves represent the output power for a resonant pump laser ($\Delta_2 = 0$) at different conditions of the cavity losses and the medium gain. The gain on the 0–1 transition with the forward-backward anisotropy has an awkward expression, but in the analysis of [20] a SW gain parameter was introduced, appropriate to the case of $\gamma_0 \gg \gamma_1, \gamma_2$ and weak pumping on the 2–0 transition. We have classified our numerical results introducing the following laser parameter:

$$C = \frac{\pi^{3/2}\mu_{10}^2 N_2^0 \gamma_0 \gamma_2 Q}{\hbar k_1 u \gamma_{02}^2} \frac{k_1^2}{(k_1^2 - k_2^2)} \frac{G}{1+G}, \tag{26}$$

where, as introduced in Sect. 2.1 above, $G = 4(\beta^-)^2/\gamma_0\gamma_2$ is the pump saturation parameter. At low G values the C parameter is equivalent to the SW gain parameter introduced in [20] multiplied by the cavity losses. The G dependence in the C definition reproduces the dependence of the χ_1 susceptibility obtained in the numerical results corresponding to threshold conditions ($\alpha^+ = \alpha^- \simeq 0$). The C parameter represents a generalization, to the three-level Raman laser, of the laser parameter introduced in the two-level laser theory [24] that is equal to 1 at the laser threshold. In the case of Fig. 4, where the hypothesis of $\gamma_0 \gg \gamma_1, \gamma_2$ is not satisfied, the threshold condition is $C = 1.27$ and the different curves are obtained for C values in the 3–7 range.

The curves of Fig. 4 have a frequency tuning determined by the Doppler width of the transition and by the parameter $(k_1 - k_2)/k_1$, but at large pump intensities they present a central dip. The theoretical treatment of [20], based on a perturbation approach and neglecting the high-order saturation effects, interpreted this dip as the simultaneous saturation of the $v = 0$ absorbers by the (β^-, α^-) and (β^-, α^+) two-photon 2–1 processes, with a width $(\gamma_1 + \gamma_2)/2$. However other saturation processes may contribute to the dip formation, and the Lamp dip process, i.e. the population saturation of the 0–1 transition, is an important one. The width of the Lamp dip, for the parameters of the experiment reported above, is comparable to the two-photon width. Making use of the matrix fraction solution we have calculated the dip width on the two limiting cases of large γ_0 or γ_{12} rates, i.e. when the Raman scattering or the Lamp dip are respectively the only existing processes, and we have verified that for the parameters introduced in the numerical results of Fig. 4 the Raman process is dominant in the dip formation. Thus our treatment provides for the experimental features a precise description that could not be obtained through the perturbative analysis of [20].

3. Conclusions

For a three-level system interacting with two electromagnetic fields (in a arbitrary combination of SW and TW) the density matrix solution has been expressed through matrix continued fractions. By assuming that the k_1 and k_2 wavenumbers of the fields are in the ratio of two a and b integer numbers, the matrix dimension results four times the largest one between the a and b numbers.

It is clear that except the particular cases with a and b very low integers the matrix continued fraction solution for two SW becomes very involved and requires a large amount of computer time. However the numerical analysis of simple configurations, e.g. $k_1 = k_2/2$, etc., will provide useful information on the most general cases.

Furthermore several important cases of the three-level spectroscopy are solved through four-dimension matrices, as shown in our detailed numerical analysis. On the basis of this formalism we have treated configurations of SW electromagnetic fields with $k_1 = k_2$ in infrared spectroscopy within molecular vibrational transitions and in two-photon spectroscopy on molecular electronic spectra. The four-dimension solution applies also to the case of a SW plus TW configuration, as in the TW laser pumping combined with a SW laser oscillation on an adjacent transition occurring in infrared transitions of neon atoms. The main features in the lineshapes of absorption or emission spectra observed in the experiments involving these configurations have been obtained and unexplored features have been presented. Thus the theoretical treatment of this paper provides an appropriate description for analysing or predicting lineshapes appearing in a large variety of experiments in nonlinear spectroscopy of three-level systems.

Acknowledgements. The authors are grateful to F. Laguarta for assistance in a part of the computer work.

Appendix

The elements of the 4×4 matrices F_q^0, $G_q^{\pm 1}$, $H_q^{\pm 1}$, and $K_q^{\pm 1}$ appearing in (16) verify useful relations based on the symmetry condition (13). If we define the following permutation σ:

(1,2); (3,4)

it results that for any integer q:

$$\begin{aligned} F_q^0(i,j) &= [F_{-q}^0(\sigma(i),\sigma(j))]^* \\ G_q^1(i,j) &= [G_{-q}^{-1}(\sigma(i),\sigma(j))]^* \\ H_q^1(i,j) &= [H_{-q}^{-1}(\sigma(i),\sigma(j))]^* \\ K_q^1(i,j) &= [K_{-q}^{-1}(\sigma(i),\sigma(j))]^* . \end{aligned} \tag{A.1}$$

Moreover if we introduce the following permutation π for indices and Rabi frequencies:

$$(1,2)\,; \quad (3,4)\,; \quad (a,b)\,; \quad (\alpha,\beta)$$

it results

$$\begin{aligned} H_q^1(i,j) &= \pi[G_q^1(\pi(i),\pi(j))] \\ F_q^0(i,j) &= \pi[F_q^0(\pi(i),\pi(j))] . \end{aligned} \tag{A.2}$$

Thus the following matrix elements are obtained

$$G_q^1(1,1) = \alpha^+\alpha^-(M_1^q + M_0^q)(L_{10}^{q+a} + L_{01}^{q+a})$$

$$G_q^1(1,4) = -\alpha^+\beta^-[(M_1^q + M_0^q)L_{01}^{q+a} + M_1^q L_{20}^{q+b}]$$

$$G_q^1(2,1) = \alpha^+\alpha^- M_2^q(L_{01}^{q+a} + L_{10}^{q+a})$$

$$G_q^1(2,4) = -\alpha^+\beta^-[(M_2^q + M_0^q)L_{20}^{q+b} + M_2^q L_{01}^{q+a}]$$

$$G_q^1(3,1) = \alpha^+\beta^- L_{10}^{q+a} L_{12}^{q+a-b}$$

$$G_q^1(3,2) = \alpha^+\beta^- L_{02}^{q+2a-b} L_{12}^{q+a-b}$$

$$G_q^1(3,3) = -\alpha^+\alpha^- L_{02}^{q+2a-b} L_{12}^{q+a-b}$$

$$G_q^1(4,4) = -\alpha^+\alpha^- L_{20}^{q+b} L_{21}^{q-a+b}$$

$$K_q^1(1,4) = -\alpha^+\beta^+[(M_1^q + M_0^q)L_{01}^{q+a} + M_1^q L_{20}^{q-b}]$$

$$K_q^1(2,4) = -\alpha^+\beta^+[M_2^q L_{01}^{q+a} + (M_2^q + M_0^q)L_{20}^{q-b}]$$

$$K_q^1(3,1) = \alpha^+\beta^+ L_{10}^{q+a-2b} L_{12}^{q+a-b}$$

$$K_q^1(3,2) = \alpha^+\beta^+ L_{02}^{q+2a-b} L_{12}^{q+a-b}$$

$$\begin{aligned} F_q^0(1,1) = {} & M_0^q M_1^q + \Gamma_{01} M_1^q + (\Gamma_{10} + \Gamma_{12}) M_0^q \\ & + (M_1^q + M_0^q)[(\alpha^+)^2(L_{10}^{q-a} + L_{01}^{q+a}) + (\alpha^-)^2(L_{10}^{q+a} \\ & + L_{01}^{q-a})] \end{aligned}$$

$$\begin{aligned} F_q^0(1,2) = {} & \Gamma_{02} M_1^q - \Gamma_{12} M_0^q + M_1^q[(\beta^+)^2(L_{20}^{q-b} + L_{02}^{q+b}) \\ & + (\beta^-)^2(L_{20}^{q+b} + L_{02}^{q-b})] \end{aligned}$$

$$F_q^0(1,3) = -\alpha^-\beta^-[(M_1^q + M_0^q)L_{10}^{q+a} + M_1^q L_{02}^{q-b}]$$

$$F_q^0(1,4) = -\alpha^-\beta^-[(M_1^q + M_0^q)L_{01}^{q-a} + M_1^q L_{20}^{q+b}]$$

$$F_q^0(3,1) = \alpha^-\beta^- L_{10}^{q+a} L_{12}^{q+a-b}$$

$$F_q^0(3,2) = \alpha^-\beta^- L_{02}^{q-b} L_{12}^{q+a-b}$$

$$\begin{aligned} F_q^0(3,3) = {} & -1 - L_{12}^{q+a-b}[(\alpha^+)^2 L_{02}^{q+2a-b} + (\alpha^-)^2 L_{02}^{q-b} \\ & + (\beta^+)^2 L_{10}^{q+a-2b} + (\beta^-)^2 L_{10}^{q+a}] . \end{aligned}$$

The remaining matrix elements, not defined by (A.1, 2), are identically zero.

The coefficients A_i and B_i appearing in (18) are defined by:

$$A_1 = \Gamma_0(\Gamma_1 + \Gamma_{01} + \Gamma_{21}) + \Gamma_1(\Gamma_{10} + \Gamma_{20} - \Gamma_{02})$$

$$A_2 = \Gamma_2\Gamma_{01} - \Gamma_0\Gamma_{21}$$

$$B_1 = \Gamma_1\Gamma_{02} - \Gamma_0\Gamma_{12}$$

$$B_2 = \Gamma_0(\Gamma_2 + \Gamma_{02} + \Gamma_{12}) + \Gamma_2(\Gamma_{20} + \Gamma_{10} - \Gamma_{01}) .$$

References

1. For reviews see V.S. Letokhov, V.P. Chebotayev: *Nonlinear Laser Spectroscopy*, Springer Ser. Opt. Sci. **4** (Springer, Berlin, Heidelberg, New York 1977)
   V.P. Chebotayev: In *Coherent Nonlinear Optics*, ed. by M.S. Feld, V.S. Letokhov, Topics Current. Phys. **21** (Springer, Berlin, Heidelberg, New York 1980) pp. 59–109
2. E. Kyrölä, R. Salomaa: Appl. Phys. **20**, 339 (1979)
3. A. Schabert, R. Keil, P.E. Toschek: Opt. Commun. **13**, 265 (1975)
4. J.L. Picqué, J. Pinard: J. Phys. B **9**, L 77 (1976)
5. P. Cahuzac, R. Vetter: Phys. Rev. A **14**, 270 (1976)
6. R. Wellegehausen, H. Heitmann: Appl. Phys. Lett. **34**, 44 (1979)
7. J. Reid, T. Oka: Phys. Rev. Lett. **38**, 67 (1977)
8. J.P. Woerdman, M.F.H. Schuurmans: Opt. Commun. **21**, 243 (1977)
9. M. Himbert, S. Reynaud, J. Dupont-Roc, C. Cohen-Tannoudji: Opt. Commun. **30**, 184 (1979)
10. J. Balias, W.J. Firth, P.E. Toschek: Opt. Commun. **36**, 317 (1981)
11. S. Stenholm, W.E. Lamb, Jr.: Phys. Rev. **181**, 618 (1969)
12. B.J. Feldman, M.S. Feld: Phys. Rev. A **1**, 1375 (1970)
13. J. Hambene, M. Sargent III: Phys. Rev. A **13**, 784 and 797 (1976)
    M. Sargent III, P.E. Toschek, H.G. Danielmeyer: Appl. Phys. **11**, 55 (1976)
    M. Sargent III, P.E. Toschek: Appl. Phys. **11**, 107 (1976)
14. A. Bambini: Phys. Rev. A **14**, 1479 (1976)
15. A. Bambini, M.A. Zoppi: Phys. Lett. **59** A, 379 (1976)
16. B.J. Feldman, M.S. Feld: Phys. Rev. A **5**, 899 (1972)
17. A.H. Paxton, P.W. Milonni: Opt. Commun. **34**, 111 (1980); Phys. Rev. A **26**, 1549 (1982)
18. E. Kyrölä, R. Salomaa: Phys. Rev. A **23**, 1874 (1981).
19. P.F. Liao, J.B. Bjorkholm, P.R. Berman: Phys. Rev. A **20**, 1489 (1979); A **21**, 1927 (1980)
20. I.M. Beterov, Yu. A. Matyugin, V.P. Chebotayev: JETP **37**, 756 (1973)
    Ye.V. Baklanov, I.M. Beterov, V.P. Chebotayev, B. Ya. Dubetsky: Appl. Phys. **11**, 75 (1976)
21. R. Corbalán, G. Orriols, L. Roso, R. Vilaseca, E. Arimondo: Opt. Commun. **38**, 113 (1981)
22. L. Roso, R. Corbalán, G. Orriols, R. Vilaseca, E. Arimondo: Appl. Phys. B **31**, 115 (1983)
23. M.F.H. Schuurmans: Lett. **61** A, 445 (1977); **63** A, 25 (1977)
24. M. Sargent III, M.D. Scully, W.E. Lamb, Jr.: *Laser Physics* (Addison-Wesley, Reading, MA 1974)